Cortical and subcortical mapping of the allostatic-interoceptive system in the human brain using 7 Tesla fMRI

Jiahe Zhang[1], Danlei Chen[1], Philip Deming[1], Tara Srirangarajan[2], Jordan Theriault[3], Philip A. Kragel[4], Ludger Hartley[1], Kent M. Lee[1], Kieran McVeigh[1], Tor D. Wager[5], Lawrence L. Wald[3], Ajay B. Satpute[1], Karen S. Quigley,[1] Susan Whitfield-Gabrieli[1], Lisa Feldman Barrett[1,3,6]* & Marta Bianciardi[3,7]*

[1] Department of Psychology, Northeastern University, Boston, MA 02115
[2] Department of Psychology, Stanford University, Stanford, CA 94305
[3] Department of Radiology, Athinoula A. Martinos Center for Biomedical Imaging, Massachusetts General Hospital, Boston, MA 02139
[4] Department of Psychology, Emory University, Atlanta, GA 30322
[5] Department of Psychological and Brain Sciences, Dartmouth College, Hanover, NH 03755
[6] Department of Psychiatry, Massachusetts General Hospital, Boston, MA 02139
[7] Division of Sleep Medicine, Harvard University, Boston, MA

*L.F.B. and M.B. share senior authorship.

Corresponding Authors:
Jiahe Zhang, Department of Psychology, 125 Nightingale Hall, Northeastern University, Boston, MA 02115-5000. Email: j.zhang@northeastern.edu
Lisa Feldman Barrett, Department of Psychology, 125 Nightingale Hall, Northeastern University, Boston, MA 02115-5000. Email: l.barrett@northeastern.edu
Marta Bianciardi, Department of Radiology, Athinoula A. Martinos Center for Biomedical Imaging, Massachusetts General Hospital and Harvard Medical School, Building 149, Room 2301, 13th Street, Charlestown, MA 02129. Email: martab@mgh.harvard.edu

Author contributions: T.W., L.W., A.B.S., L.F.B. and M.B. designed research. J.Z., D.C., J. T., L.H., K.M.L, K.M., A.B.S., K.S.Q., S.W-G., L.F.B. and M.B. performed research. J.Z., D.C., P.D., T.S., L.F.B. and M.B. analyzed data and wrote the paper. All authors read and approved the paper.

Competing interest statement: The authors declare no conflict of interest.

Classification: Biological Sciences/Neuroscience

Keywords: visceromotor, interoception, viscerosensory, allostasis, default mode network, salience network

Abstract
The brain continuously anticipates the energetic needs of the body and prepares to meet those needs before they arise, called allostasis. In support of allostasis, the brain continually models the sensory state of the body, called interoception. We replicated and extended a large-scale system supporting allostasis and interoception in the human brain using ultra-high precision 7 Tesla functional magnetic resonance imaging (fMRI) (N = 90), improving the precision of subgenual and pregenual anterior cingulate topography combined with extensive brainstem nuclei mapping. We observed over 90% of the anatomical connections published in tract-tracing studies in non-human animals. The system also included regions of dense intrinsic connectivity broadly throughout the system, some of which were identified previously as part of the backbone of neural communication across the brain. These results strengthen previous evidence for a whole-brain system supporting the modeling and regulation of the internal milieu of the body.

Introduction

A brain efficiently regulates and coordinates the systems of the body as it continually interfaces with an ever-changing and only partly predictable world. Various lines of research, including tract-tracing studies of non-human animals (e.g., 1, 2), discussions of predictive processing (3–6), and research on the central control of autonomic nervous system function (7–11), all suggest the existence of a unified, distributed brain system that anticipates the metabolic needs of the body and prepares to meet those needs before they arise, a process called allostasis (10; for recent reviews, see 11, 12). Allostasis is not a condition or state of the body — it is the process by which the brain efficiently coordinates and regulates the various systems of the body (12). Just as somatosensory and other exteroceptive sensory signals are processed in the service of skeletomotor control, the brain is thought to model the internal sensory conditions of the body (i.e., the internal milieu) in the service of allostasis, a process known as interoception (15–18).

Using resting state functional magnetic resonance imaging (fMRI) in three samples totalling almost 700 human subjects scanned at 3 Tesla (19), we previously identified a distributed allostatic-interoceptive system consisting of two well-known intrinsic networks, the default mode network and salience networks, overlapping in many key cortical visceromotor allostatic regions that also serve as 'rich club' hubs that have been implicated as the "backbone" for neural communication throughout the brain (**Figure 1A**). Our investigation was guided by the anatomical tracts identified in published studies of macaques and other non-human mammals (see Table 2 in (19)). This first study was more cortically focused, examining the functional connectivity of primary interoceptive cortex spanning the dorsal mid and dorsal posterior insula (dmIns/dpIns), as well as key allostatic regions in the cerebral cortex that are directly connected to the brainstem regions that are known to be responsible for controlling the motor changes in the viscera (i.e., visceromotor cortical regions), such as the anterior midcingulate cortex (aMCC), pregenual anterior cingulate cortex (pACC), subgenual anterior cingulate cortex (sgACC), and agranular insular cortex (also known as ventral anterior insula, or vaIns, which is also posterior orbitofrontal cortex), as well as the dorsal sector of the amygdala (dAmy) containing the intercalated bodies and the central nucleus (**Figure 1A**). Our 3T analysis yielded a replicable, integrated system consisting of two well-known intrinsic networks, in addition to primary interoceptive cortex. We did explore some aspects of the system's subcortical extent, including the thalamus, hypothalamus, hippocampus, ventral striatum, periaqueductal gray (PAG), parabrachial nucleus (PBN) and nucleus tractus solitarius (NTS), all regions known to play a role in control of the autonomic nervous system, the immune system, and the endocrine system (e.g., 18–24), but our ability to more extensively map the midbrain and brainstem extents of the system were limited by our use of 3T imaging.

In the present study, we replicated and extended evidence for the allostatic-interoceptive system (**Figure 1B**) using ultra-high field (7 Tesla) MRI, which allows data acquisition with higher spatial resolution (1.1 mm isotropic), better signal-to-noise-ratio (SNR; (27–29)), and increased sensitivity in mapping functional connectivity of brainstem nuclei involved in arousal, motor and other vital processes (e.g., autonomic, nociceptive, sensory; (30, 31)). This is a particularly important effort given the increasing importance of the allostatic-interoceptive system as a tool for investigating interoception and allostasis in basic brain function both in neurotypical samples and in specific populations (e.g., (32–35)). In addition, research indicates that regions in this system are also important for a wide range of psychological domains, including cognition, emotion, pain, decision-making and perception (see Figure 5 in (19); also see (36–38)), suggesting the hypothesis that allostatic and interoceptive signals may play a more fundamental role in shaping basic brain dynamics (for discussion see (5, 39–41)).

We tested within-system functional connectivity in 90 human participants (age range = 18-40 years, mean = 26.9 years, s.d. = 6.2 years; 40 females) using a fast low-angle excitation echo-planar technique (FLEET) sequence shown to reduce artifacts and improve temporal SNR (24, 42). This approach allowed a more precise mapping of connectivity for regions with known signal issues at 3 Tesla, such as the sgACC (low SNR), amygdala (noise from adjacent veins; (43)), columns within the PAG

(noise from adjacent aqueduct), and other small structures that could be particularly influenced by partial volume effects. We took advantage of recently developed, much improved and validated in-vivo brainstem and diencephalic nuclei atlases (44–48) to guide our analysis. This was crucial because our hypotheses were specifically derived from published tract-tracing studies of macaques and other non-human mammals that establish structural pathways carrying ascending interoceptive signals from the periphery, for example via the vagus nerve, to subcortical and cortical regions of the allostatic-interoceptive system (**Supplementary Table 1**). Extending (19), we more extensively examined the intrinsic connectivity of subcortical nuclei such as mediodorsal thalamus (mdThal), hypothalamus, dorsal amygdala, hippocampus, ventral striatum, PAG, PBN and the NTS (in the medullary viscero-sensory-motor nuclei complex; VSM), in addition to considering the connectivity of dorsal raphe (DR), substantia nigra (SN), ventral tegmental area (VTA), locus coeruleus (LC), superior colliculus (SC), and lateral geniculate nucleus (LGN). The DR, SN, VTA and LC are midbrain and pontine monoamine-producing nuclei that contribute to relaying the body's metabolic status to the cortex (49). The SC and LGN are not traditionally considered to be directly involved in interoception and allostasis, but they share anatomical connections with key visceromotor regulation regions in the system (see **Supplementary Table 1**; (50–55)). For example, neurons in the intermediate and deep layers of the SC are connected to aMCC (56), hypothalamus (57, 58) and PAG (59), and have been directly implicated in skeletomotor (60, 61) and visceromotor (62, 63) actions that facilitate approach or avoidance behaviors. The SC is also thought to be a major point of sensory-motor integration and is associated with affective feelings (64, 65). The LGN receives interoceptive inputs from the PAG (52) and PBN (55, 66, 67), and shares monosynaptic connections with the hypothalamus (68) and pACC (69). We also examined connectivity patterns for subregions of the PAG, hippocampus and SC rather than as a single ROI as in (19) given their functional heterogeneity (70, 71) and differential involvement in allostasis (e.g., (72–74)).

Results

We used a bootstrapping strategy to identify weak but reliable signals that are important when examining cortico-subcortical connections in brain-wide analyses. For each of 1000 iterations, we randomly resampled 80% of the subjects ($N = 72$) and identified, for each seed region, BOLD correlations for all voxels in the brain that survived a voxel-wise threshold of $p < .05$. We calculated discovery maps for each seed region that included both cortical and subcortical connections. We calculated the similarities in the spatial topography among all the maps and subjected each resulting similarity matrix to *k*-means clustering analysis to characterize the allostatic-interoceptive network. We expected stronger connectivity among cortical seeds compared to among subcortical seeds due to the latter's noisier time courses and potential partial volume effects, which would result in lower correlations for smaller regions.

Cortico-cortical intrinsic connectivity. We first examined the hypothesized functional connectivity according to published anatomical connections. As expected, we successfully replicated all of the cortico-cortical connections we previously observed with 3 Tesla imaging (**Figure 2, Supplementary Table 1**) (19). We additionally observed reciprocal intrinsic connectivity (i.e., connectivity map of one region includes a cluster in the other region and vice versa) between the lvAIns and pACC, between the sgACC and aMCC, and between the dmIns and portions of cingulate cortex (sgACC, pACC) (**Figure 2A**; see **Supplementary Figure 1** for *t*-value map based on full group), extending the allostatic-interoceptive system to include more of the anatomical connections documented in tract-tracing studies in non-human mammals (75–78). All of these observations were confirmed by seed-to-seed connectivity strength calculation (**Figure 2B**). Using evidence from the cortical maps and the seed-to-seed connectivity matrices, we confirmed 100% of the monosynaptic cortico-cortical connections documented in published tract-tracing studies in non-human animals.

Next, we binarized the cortical connectivity maps for all cortical seeds ($p < 0.05$) and computed their conjunction to identify connecting cortical regions (**Figure 2C**). A *k*-means clustering analysis

(optimal $k = 2$ based on the Calinski-Harabasz Criterion (79)) on the cortical maps replicated (19), such that the system included two subsystems, one corresponding to the default mode network (i.e., the dorsomedial prefrontal cortex, posterior cingulate cortex (PCC), and dorsolateral prefrontal cortex) and the other corresponding to the salience (i.e., anterior to MCC, anterior insula, supramarginal gyrus, supplementary motor area) and somatomotor networks (i.e., M1, S1, superior temporal gyrus; see details in **Supplementary Figure 2**). This procedure also allowed us to discover any regions that might be reliably included in the intrinsic connectivity of the system. We replicated all the connecting 'hub' regions reported at 3 Tesla in (19) (i.e., portions of anterior/posterior midcingulate cortex, inferior frontal gyrus, ventral anterior insula, dorsal posterior insula, temporal pole, inferior temporal gyrus, superior temporal sulcus, parahippocampal gyrus, and cuneus) with the exception of medial postcentral gyrus. We also newly identified as allostatic-interoceptive system 'hubs' the entire anterior cingulate cortex (including subgenual and pregenual extents), PCC, a greater extent of the insula (including mid insula; mIns), as well as some portions of medial superior frontal gyrus (SFG) and middle frontal gyrus (MFG). A majority of the allostatic-interoceptive system's connecting hubs have been identified as members of the 'rich club' in the connectomics literature, defined as high-degree nodes showing denser interconnections among themselves than are lower degree nodes (80). The rich club hubs play a key role in global information integration across the brain and therefore may serve as the backbone for global communication in the brain (81), suggesting that allostatic and interoceptive processes may be at the core of the brain's computational architecture.

Subcortico-cortical intrinsic connectivity. In a new analysis enabled by newly delineated subcortical seeds (45, 48, 82) that was not possible at 3 Tesla (19), we assessed subcortico-cortical connectivity by visually inspecting cortical discovery maps of the subcortical seeds to confirm topography (**Figure 3A**; see **Supplementary Figure 3** for *t*-value map based on full group) and calculating seed-to-seed connectivity to quantify strength of connection (**Figure 3B**). Combining evidence from the cortical maps and seed-to-seed connectivity matrix, we confirmed 94% of the monosynaptic subcortico-cortical connections predicted from non-human tract-tracing studies (**Supplementary Table 1**). There were three exceptions: we did not observe significant, positive functional connectivity between PAG and dmIns/dpIns, hypothalamus and dmIns/dpIns, or PBN and sgACC, despite known anatomical connections (see **Supplementary Table 1**; (83, 84)). In some instances, averaged time courses between seeds did not correlate significantly (i.e., *gray* squares in **Figure 3B**, e.g., DR-sgACC), but connectivity clusters could nonetheless be observed in the maps (e.g., sgACC cluster in DR-seeded map). Such discrepancies can result from noisy signals within an ROI or specific sub-portions of an ROI showing significant connectivity. We tested specificity of the allostatic-interoceptive network using a region of superior parietal lobule not known for visceromotor function (19). This region only showed consistent functional connectivity to the SC (85), VSM, the hippocampus and the amygdala (**Supplementary Table 2**).

As with the cortico-cortical analyses, we conjoined the binarized discovery subcortico-cortical maps ($p < 0.05$) to identify the overlapping cortical connectivity between subcortical seeds (**Figure 3C**). Subcortically seeded maps showed connecting regions in hypothesized cingulate and insular regions as well as some parts of the MFG and cuneus. We examined a range of k values that showed similarly optimal Calinski-Harabasz Criterion ($k = 2$ to 9) (see **Supplementary Methods**). We retained $k = 3$ for its interpretability. All three clusters included cortical nodes from the default mode and salience networks. Cluster 1 included discovery maps from seeds in the lower brainstem (LC, PBN, VSM), and primarily showed connectivity to the posterior cingulate cortex, supramarginal gyrus and some medial and lateral occipital regions (**Supplementary Figure 4**). Cluster 2 included discovery maps from seeds in the upper brainstem (PAG, DR) and the hypothalamus, and showed connectivity to the aMCC and parahippocampal gyrus. Cluster 3 included discovery maps from larger seeds in the mdThal, LGN, hippocampus, dAmy, NAcc, SC, SN and VTA, and showed widespread connectivity to the dorsomedial prefrontal cortex,

cingulate cortices (sgACC, pgACC, aMCC, isthmus), supplementary motor area, cuneus, insula (anterior, mid and posterior), superior frontal gyrus, central sulcus, and angular gyrus.

Subcortico-subcortical intrinsic connectivity. With our newly delineated subcortical seeds (45, 48, 82), we also assessed subcortico-subcortical connectivity by visually inspecting subcortical maps of the subcortical seeds to confirm topography (**Figure 4A**) and by calculating functional connectivity between all subcortical seeds to quantify strength of connection (**Figure 4B**). Again, this analysis was not possible with 3 Tesla scanning as in (19). We confirmed 96% of the monosynaptic subcortico-subcortical connections that were identified in published, tract-tracing studies on non-human animals (**Supplementary Table 1**). There were three exceptions: we did not observe significant, positive functional connectivity between hypothalamus and PBN, hypothalamus and LC, or hypothalamus and VSM (including NTS), despite known anatomical connections (see **Supplementary Table 1**). In one case, averaged timecourses between the VSM and NAcc seeds did not correlate significantly (**Figure 4B**; see *gray* square in matrix), but bilateral NAcc clusters could nonetheless be observed in the VSM-seeded map. As in the subcortico-cortical maps, such discrepancies can result from noisy signals within an ROI or specific sub-portions of an ROI showing significant connectivity. Seed-to-seed connectivity strength between PAG subregions and other subcortical ROIs is displayed in **Supplementary Figure 5**. Seed-to-seed connectivity strength between hippocampal subregions and other subcortical ROIs is displayed in **Supplementary Figure 6**. Seed-to-seed connectivity strength between layers of the SC and other subcortical ROIs is displayed in **Supplementary Figure 7**. Conjoined binarized subcortical discovery maps ($p < 0.05$) indicated that all but four subcortical seeds showed overlapping connectivity: connecting regions were identified in the mdThal, LGN, hippocampus, dAmy, NAcc, PAG, DR, SC, SN and VTA but hypothalamus, PBN, LC and VSM showed less widespread and dense connectivity throughout subcortical seeds (**Supplementary Table 3**). K-means clustering analysis ($k = 3$) on the subcortical discovery maps from subcortical seeds yielded an almost identical solution as their cortical connectivity maps.

The allostatic-interoceptive system. We observed dense interconnectivity between all the cortical and subcortical seeds included in our analysis (**Figure 5A**). Conjoined binarized discovery maps ($p < 0.05$) across both cortical and subcortical extents converged in the hypothesized allostatic-interoceptive system (**Figure 5B**).

Discussion

Ultra-high field 7 Tesla fMRI with 1.1-mm isotropic voxel resolution combined with newly delineated 7 Tesla brainstem and diencephalic parcellations (44–48) revealed both cortical and subcortical components of an integrated allostatic-interoceptive system in humans consisting of two overlapping subsystems. Our original study using 3 Tesla fMRI (19) used 10-minute resting state scans in two subsamples of 270-280 participants each, plus a third sample of N = 41, whereas the present study involved a greater duration of resting state scan time (30 minutes total) in a sample of 90 participants. Using functional connectivity among seven cortical ROIs and 14 subcortical ROIs in humans, we verified over 90% of the anatomical connections identified in published tract-tracing studies of macaques and other non-human mammals. Our current 7 Tesla findings revealed reciprocal connectivity between sgACC/pACC and dmIns/dpIns regions previously unreported in 3 Tesla functional connectivity studies of the ACC (86–90) and the insula (91–94). The improvement in sgACC connectivity, in particular, was expected at 7 Tesla, as this region is part of the medial/orbital surface that is typically susceptible to low SNR, partial volume effects and physiological aliasing. In the current study, these effects were mitigated by higher resolution image acquisition at 7 Tesla, minimal smoothing, and more precise nuisance regression using signals from individual ventricles. We also expanded observations of the subcortical extents of the system.

Several subcortical nodes (i.e., mdThal, LGN, hippocampus, dAmy, NAcc, SC, SN and VTA) showed robust connectivity with all cortical nodes whereas the smaller brainstem nuclei (i.e., PAG, DR, PBN, LC and VSM (including the NTS)) showed weaker but reliable connectivity to these nodes, consistent with other studies that examined a subset of the nodes as seeds at 3 Tesla (e.g., (49)) and 7 Tesla (e.g., (30, 95, 96)). We also observed reliable connectivity between regions that have not yet been documented as having monosynaptic connections in previous tract-tracing studies. For example, the LGN has virtually no monosynaptic connectivity with cortical nodes of the allostatic-interoceptive system according to tract-tracing studies (except for modest projections to the pACC (97)), yet we observed reliable functional connectivity between the LGN and the aMCC, mvAIns, and pACC. The LGN receives interoceptive input (67) and there is some evidence that interoceptive signals gate visual sensory sampling (98), suggesting that LGN functional connectivity with other nodes of the allostatic-interoceptive system might reflect polysynaptic connections that are functionally meaningful. In our study, the observation of a broad allostatic-interoceptive system is consistent with the confirmed monosynaptic connections between the *a priori* ROIs and the understanding that functional connectivity may reflect both monosynaptic and polysynaptic connections (99).

The connecting 'hub' regions of the allostatic-interoceptive system observed at 7 Tesla covered *all* hypothesized cortical regions of interest, including the full extent of primary interoceptive cortex (dpIns, dmIns; (15)) and the primary visceromotor regions (vAIns, sgACC, pACC and aMCC; (100)). Several other connecting 'hub' regions (MCC, PCC, IFG, PHG, STG) were also observed and we confirmed their anatomical connections to documented allostatic regions in non-human animals. The remaining connecting regions (i.e., MFG, SFG, isthmus of the cingulate, cuneus) have not been documented as having monosynaptic anatomical connections to our subcortical and cortical seed regions – their functional connectivity may reflect polysynaptic connections or novel connections in humans. Importantly, most of the additional connecting regions observed at 7 Tesla (i.e., pACC, PCC, isthmus cingulate, SFG, MFG and mIns; except the sgACC) belong to the 'rich club' (the most densely interconnected regions in the cortex and thought to serve as the "backbone" that synchronizes neural communication throughout the brain; (105)), consistent with the hypothesized central role of the allostatic-interoceptive system as a high-capacity "backbone" for integrating information across the entire brain (106).

The results of this study have several important functional implications. First, a number of brain regions within the allostatic-interoceptive network most likely play an important role in coordinating and regulating the systems of the body even though they are involved in other psychological phenomena. For example, the SC is typically studied for visuomotor functioning in humans but has been shown to be important for approach and avoidance behavior as well as the accompanying changes in visceromotor activity in non-human mammals (e.g., 62, 63, 107) via anatomical connections to ACC (50) and hypothalamus (51). Similarly, the hippocampus is usually considered central to memory function, but evidence from non-human animals indicates that the hippocampus also plays a role in the regulation of feeding behaviors and in interoception-related reward signals (108–113). There is also circumstantial evidence that interoceptive signals, relayed from the vagus nerve to the hippocampus via the NTS and septal nuclei, may play a role in event segmentation (114, 115). Furthermore, the LGN is usually considered part of the visual pathway that relays visual information from the retina and the cerebral cortex. However, the current functional connectivity findings are consistent with tract-tracing evidence showing LGN's monosynaptic connections with cortical (e.g., pACC (69)) and subcortical visceromotor structures (e.g., hypothalamus (68), PAG (52), and PBN (116)), suggesting a role for facilitating communication among brain structures implicated in bodily regulation, in addition to its role in integrating interoceptive and visual signals (39). The broad functional connectivity profile of the LGN is also consistent with evidence of tracts between the LGN and other hypothesized regions of the allostatic-

interoceptive network such as the hippocampus, amygdala, DR, SC, SN, and LC (**Supplementary Table 1**).

Second, both the default mode and salience networks have been functionally implicated in cardiovascular regulation as well as other aspects of allostasis (9, 117, 118), and they have also been implicated in mental and physical illness and their comorbidities (e.g., (119, 120)). Not surprisingly, psychiatric illnesses (e.g., depression (121, 122), schizophrenia (123, 124)), neurodevelopmental illnesses (e.g., sensory processing disorder/autism spectrum disorder (125, 126)), neurodegenerative illnesses (e.g., dementia/Alzheimer's disease (127, 128), Parkinson's disease (129, 130)) and physical illnesses (e.g., heart disease (131), chronic pain (132)) present with symptoms related to altered interoception or visceromotor control, and some of these symptoms are transdiagnostic (133–135). Moreover, interoceptive and visceromotor symptomatology is often accompanied by altered neurobiology (e.g., volume, structural connectivity, functional connectivity, evoked potential, task activation) in the allostatic-interoceptive system (e.g., depression: (136, 137); autism: (138); dementia: (33, 127, 128); chronic pain: (139); transdiagnostic: (140–143)). In addition, there is evidence showing that psychological therapies targeting interoceptive processes (144) and neuromodulations targeting distributed regions within the allostatic-interoceptive system (145, 146) may be effective transdiagnostic interventions. Taken together, these findings suggest that altered function of the allostatic-interoceptive system may be a transdiagnostic feature of mental and physical illness that holds promising clinical utility. More fundamentally, the system identified in this paper provides a scientific tool for integrating studies across psychological and illness domains in a manner that will speed discovery, the accumulation of knowledge and, potentially, strategies for more effective treatments and prevention.

Finally, the findings reported here are consistent with the growing body of evidence that a number of subcortical and cortical brain regions are important during both the regulation of bodily functions and during cognitive phenomena, calling into question their functional segregation (147–149). Our findings suggest that the default mode and salience networks may be concurrently coordinating, regulating and representing organs and tissues of the internal milieu at the same time that they are engaged in a wide range of tasks spanning cognitive, perceptual, emotion and action domains (see Figure 5 in (19)) (38, 150–154). Therefore, our results, when situated in the broader published literature, suggest that the default mode and salience networks create a highly connected functional ensemble for integrating information across the brain, with interoceptive and allostatic signaling at the core. Regulation of the body has been largely ignored in the neuroscientific study of the mind, in part because much of interoceptive modeling occurs outside of human awareness (18, 134).

Several limitations within the current study should be addressed in future studies. First, we did not validate the connectivity strength within the allostatic-interoceptive network against signal-based measures of interoception (e.g., heart-beat evoked potentials), although there is growing evidence that even at rest, limbic regions of the brain continually issue allostatic control signals and there should be synchronous relationships between resting state BOLD signals and electrical signals from visceromotor movements (155). Second, we did not fully monitor participants' wakefulness (e.g., via video recording) during the three ten-minute resting state scans. The default mode and salience networks are present during sleep (156), although the strength of within-network functional connectivity has been shown to vary (with evidence of both stronger and weaker connectivity) as a function of wakefulness (157–160). Third, we did not map every relevant subcortical area that may be involved in allostasis or interoception. For example, opportunities for further research include septal nuclei (with direct projections to limbic regions such as the hippocampus and implicated in temporal control of neurons that make up the allostatic-interoceptive network; (161, 162)), circumventricular organs (e.g., area postrema with unique access to peripheral signaling molecules via its permeable blood-brain barrier; (163, 164)), and motor brainstem nuclei (e.g., dorsal motor nucleus of the vagus and nucleus ambiguus whose neurons give rise to the efferent vagus nerve; (165, 166)). As several of the known anatomical connections of the hypothalamus were not observed, further investigation of hypothalamic functional connectivity is warranted. Further investigation should use different hypothalamic nuclei or subregions as seeds may given functional heterogeneity in

relation to allostatic processes (167, 168) . The cerebellum is also likely involved in allostasis and interoception (169, 170).

Online Methods

Participants and MRI acquisition. We recruited 140 native English-speaking adults, with normal or corrected-to-normal vision, and no history of neurological or psychiatric conditions. All participants provided written informed consent in accordance with the guidelines set by the institutional review board of Massachusetts General Hospital. Forty-nine participants were excluded from the current analysis (19 withdrew prior to the MRI session, three withdrew during MRI acquisition due to discomfort, six did not complete scans due to online scan reconstruction failure, three did not complete scans due to time constraint, four were excluded due to other technical issues during acquisition, 10 were excluded due to scanner sequence error, four were excluded due to corrupted MRI data that could not be processed and one was excluded due to excessive artifacts in the structural scan). This resulted in a final sample of 90 participants (26.9 ± 6.2 years old; 40 females, 50 males). MRI data were acquired using a 7 Tesla scanner (Magnetom, Siemens Healthineers, Erlangen, Germany) with a 32-channel phased-array head coil and personalized padding to achieve a tight fit. Participants completed a structural scan, three resting state scans of 10 minutes each, three diffusion-weighted scans, as well as other tasks unrelated to the current analysis. At the beginning of each resting state scan, participants were instructed to keep their eyes open and indicated their readiness to start the scan via button press. MRI parameters are detailed in SI.

Preprocessing of fMRI data. The preprocessing pipeline began with reorientation, slice timing correction, concatenation of all three resting state runs, coregistration to the structural T_1-weighted image, and motion correction (framewise displacement mean = 0.17, s.d. = 0.14, with 98.7% of frames showing sub-voxel motion; (171)). We then conducted nuisance regression to remove physiological noise due to motion (six parameters measuring rotation and translation), as well as due to non-BOLD effects evaluated in the white matter, ventricular cerebrospinal fluid, and the cerebral aqueduct. We then conducted temporal filtering and normalization. Finally, we performed conversion to Freesurfer orientation/dimensions, detrending, spatial smoothing (1.25mm), and resampling to cortical surfaces. Preprocessing details are provided in SI.

Functional Connectivity Analysis. Seven cortical seeds (4mm-radius spheres) were defined based on previous fMRI studies of interoception using the procedure outlined in (172). The 14 subcortical seeds were defined based on the Brainstem Navigator toolkit (https://www.nitrc.org/projects/brainstemnavig/) (e.g., (95)), CANLAB Combined Atlas 2018 (github.com/canlab), and Freesurfer segmentation (e.g., (173)). See **Supplementary Methods** for details about seed definition. We randomly resampled 80% of the sample ($N = 72$) 1000 times. In each iteration, for each seed, we estimated cortical connectivity using Freesurfer-based analysis procedure as outlined in (19). This yielded final group maps that showed regions whose fluctuations significantly correlated with the seed's fMRI time series, which were binarized to retain positive connectivity surviving the threshold of $p < .05$ and summed across 1000 iterations to obtain 'bootstrapped connectivity' maps. We also quantified seed-to-seed functional connectivity by computing Pearson's correlation coefficient between all pairs of ROIs and applying the Fisher's *r*-to-*z* transform. Significance at the group level was assessed with a two-tailed one-sample t test.

Connecting Regions and K-Means Cluster Analysis. To visualize the connecting 'hub' regions, we conjoined binarized functional connectivity maps ($p < 0.05$) for all seeds. To replicate the previously discovered two-subsystem distinction within the allostatic-interoceptive network (19), we first computed a similarity matrix capturing pairwise η^2 (174) between the un-thresholded bootstrapped group maps of cortical seeds and then applied k-means clustering algorithm (*kmeans*, MATLAB) with a range of k between 2-10 (for each k, we tested 10 initializations with new centroid positions, each with a maximum of 1000 iterations to find the lowest local minimum for sum of distances). We evaluated the optimal k

using the Calinski-Harabasz Criterion (79). To visualize each subsystem, we binarized the group connectivity maps ($p < 0.05$) and calculated the conjunction between maps within the same cluster.

Data and Code Accessibility. Raw and preprocessed data can be found at: https://openneuro.org/datasets/ds005747. Analysis outputs and codes can be found at: https://github.com/jiahez/7-Tesla-Allostatic-Interoceptive-System.

Acknowledgments:
This work was supported by grants from the National Institutes of Health (NCI U01 CA193632, R01 AG071173, R01 MH109464, R01 MH113234, NIDCD R21 DC015888, NIBIB K01 EB019474, and NIA R01 AG063982), the National Science Foundation (BCS 1947972), the U.S. Army Research Institute for the Behavioral and Social Sciences (W911NF-16-1-019), and the Unlikely Collaborators Foundation. The views, opinions, and/or findings contained in this review are those of the authors and shall not be construed as an official Department of the Army position, policy, or decision, unless so designated by other documents, nor do they necessarily reflect the views of the Unlikely Collaborators Foundation.

References

1. H. Barbas, N. Rempel-Clower, Cortical structure predicts the pattern of corticocortical connections. *Cerebral Cortex* **7**, 635–646 (1997).

2. D. Ongür, A. T. Ferry, J. L. Price, Architectonic subdivision of the human orbital and medial prefrontal cortex. *J Comp Neurol* **460**, 425–449 (2003).

3. L. F. Barrett, W. K. Simmons, Interoceptive predictions in the brain. *Nat Rev Neurosci* **16**, 419–429 (2015).

4. K. Friston, T. FitzGerald, F. Rigoli, P. Schwartenbeck, G. Pezzulo, Active Inference: A Process Theory. *Neural Computation* **29**, 1–49 (2017).

5. J. B. Hutchinson, L. F. Barrett, The Power of Predictions: An Emerging Paradigm for Psychological Research. *Current Directions in Psychological Science* **28**, 280–291 (2019).

6. H. Straka, J. Simmers, B. P. Chagnaud, A New Perspective on Predictive Motor Signaling. *Curr Biol* **28**, R232–R243 (2018).

7. E. E. Benarroch, The Central Autonomic Network: Functional Organization, Dysfunction, and Perspective. *Mayo Clinic Proceedings* **68**, 988–1001 (1993).

8. P. J. Gianaros, T. D. Wager, Brain-Body Pathways Linking Psychological Stress and Physical Health. *Curr Dir Psychol Sci* **24**, 313–321 (2015).

9. G. Valenza, *et al.*, The central autonomic network at rest: Uncovering functional MRI correlates of time-varying autonomic outflow. *Neuroimage* **197**, 383–390 (2019).

10. G. Valenza, F. D. Ciò, N. Toschi, R. Barbieri, Sympathetic and parasympathetic central autonomic networks. *Imaging Neuroscience* **2**, 1–17 (2024).

11. G. Valenza, L. Passamonti, A. Duggento, N. Toschi, R. Barbieri, Uncovering complex central autonomic networks at rest: a functional magnetic resonance imaging study on complex cardiovascular oscillations. *J R Soc Interface* **17**, 20190878 (2020).

12. P. Sterling, Allostasis: a model of predictive regulation. *Physiol Behav* **106**, 5–15 (2012).

13. P. Sterling, S. Laughlin, *Principles of Neural Design* (MIT Press, 2015).

14. Y. Katsumi, J. E. Theriault, K. S. Quigley, L. F. Barrett, Allostasis as a core feature of hierarchical gradients in the human brain. *Network Neuroscience* 1–56 (2022). https://doi.org/10.1162/netn_a_00240.

15. A. D. Craig, How do you feel? Interoception: the sense of the physiological condition of the body. *Nature Reviews Neuroscience* **3**, 655–666 (2002).

16. A. D. Craig, *How Do You Feel?: An Interoceptive Moment with Your Neurobiological Self* (Princeton University Press, 2014).

17. H. D. Critchley, N. A. Harrison, Visceral Influences on Brain and Behavior. *Neuron* **77**, 624–638 (2013).

18. K. S. Quigley, S. Kanoski, W. M. Grill, L. F. Barrett, M. Tsakiris, Functions of Interoception: From Energy Regulation to Experience of the Self. *Trends in Neurosciences* **44**, 29–38 (2021).

19. I. R. Kleckner, *et al.*, Evidence for a large-scale brain system supporting allostasis and interoception in humans. *Nature Human Behaviour* **1**, 1–14 (2017).

20. G. G. Berntson, S. S. Khalsa, Neural Circuits of Interoception. *Trends in Neurosciences* **44**, 17–28 (2021).

21. H. C. Evrard, The Organization of the Primate Insular Cortex. *Front. Neuroanat.* **13**, 43 (2019).

22. P. J. Gianaros, L. K. Sheu, A review of neuroimaging studies of stressor-evoked blood pressure reactivity: Emerging evidence for a brain-body pathway to coronary heart disease risk. *NeuroImage* **47**, 922–936 (2009).

23. R. M. Harper, *et al.*, fMRI responses to cold pressor challenges in control and obstructive sleep apnea subjects. *Journal of Applied Physiology* **94**, 1583–1595 (2003).

24. A. B. Satpute, P. A. Kragel, L. F. Barrett, T. D. Wager, M. Bianciardi, Deconstructing arousal into wakeful, autonomic and affective varieties. *Neuroscience Letters* **693**, 19–28 (2019).

25. T. D. Wager, *et al.*, Brain mediators of cardiovascular responses to social threat: Part I: Reciprocal dorsal and ventral sub-regions of the medial prefrontal cortex and heart-rate reactivity. *NeuroImage* **47**, 821–835 (2009).

26. M. Zunhammer, T. Spisák, T. D. Wager, U. Bingel, Meta-analysis of neural systems underlying placebo analgesia from individual participant fMRI data. *Nat Commun* **12**, 1391 (2021).

27. R. Sclocco, F. Beissner, M. Bianciardi, J. R. Polimeni, V. Napadow, Challenges and opportunities for brainstem neuroimaging with ultrahigh field MRI. *NeuroImage* **168**, 412–426 (2018).

28. A. T. Newton, B. P. Rogers, J. C. Gore, V. L. Morgan, Improving measurement of functional connectivity through decreasing partial volume effects at 7 T. *NeuroImage* **59**, 2511–2517 (2012).

29. P. A. Bandettini, R. Bowtell, P. Jezzard, R. Turner, Ultrahigh field systems and applications at 7 T and beyond: Progress, pitfalls, and potential. *Magnetic Resonance in Medicine* **67**, 317–321 (2012).

30. S. Cauzzo, *et al.*, Functional connectome of brainstem nuclei involved in autonomic, limbic, pain and sensory processing in living humans from 7 Tesla resting state fMRI. *NeuroImage* **250**, 118925 (2022).

31. J. Y. Hansen, *et al.*, Integrating brainstem and cortical functional architectures. *Res Sq* rs.3.rs-3569352 (2023). https://doi.org/10.21203/rs.3.rs-3569352/v1.

32. J. Migeot, *et al.*, Allostatic-interoceptive anticipation of social rejection. *NeuroImage* **276**, 120200 (2023).

33. A. Birba, *et al.*, Allostatic-Interoceptive Overload in Frontotemporal Dementia. *Biological Psychiatry* **92**, 54–67 (2022).

34. A. L. Ruiz-Rizzo, *et al.*, Human subsystems of medial temporal lobes extend locally to amygdala nuclei and globally to an allostatic-interoceptive system. *NeuroImage* **207**, 116404 (2020).

35. G. M. Alvarez, M. D. Rudolph, J. R. Cohen, K. A. Muscatell, Lower Socioeconomic Position Is Associated with Greater Activity in and Integration within an Allostatic-Interoceptive Brain Network in Response to Affective Stimuli. *Journal of Cognitive Neuroscience* **34**, 1906–1927 (2022).

36. L. F. Barrett, A. B. Satpute, Large-scale brain networks in affective and social neuroscience: towards an integrative functional architecture of the brain. *Current Opinion in Neurobiology* **23**, 361–372 (2013).

37. M. L. Anderson, *After Phrenology: Neural Reuse and the Interactive Brain* (MIT Press, 2014).

38. B. T. T. Yeo, *et al.*, Functional Specialization and Flexibility in Human Association Cortex. *Cereb Cortex* **25**, 3654–3672 (2015).

39. D. Azzalini, I. Rebollo, C. Tallon-Baudry, Visceral Signals Shape Brain Dynamics and Cognition. *Trends in Cognitive Sciences* **23**, 488–509 (2019).

40. R. V. Raut, *et al.*, Global waves synchronize the brain's functional systems with fluctuating arousal. *Science Advances* **7**, eabf2709 (2021).

41. I. Rebollo, C. Tallon-Baudry, The Sensory and Motor Components of the Cortical Hierarchy Are Coupled to the Rhythm of the Stomach during Rest. *J. Neurosci.* **42**, 2205–2220 (2022).

42. J. R. Polimeni, *et al.*, Reducing sensitivity losses due to respiration and motion in accelerated echo planar imaging by reordering the autocalibration data acquisition. *Magnetic Resonance in Medicine* **75**, 665–679 (2016).

43. R. N. Boubela, *et al.*, fMRI measurements of amygdala activation are confounded by stimulus correlated signal fluctuation in nearby veins draining distant brain regions. *Sci Rep* **5**, 10499 (2015).

44. M. Bianciardi, *et al.*, Toward an In Vivo Neuroimaging Template of Human Brainstem Nuclei of the Ascending Arousal, Autonomic, and Motor Systems. *Brain Connect* **5**, 597–607 (2015).

45. M. G. García-Gomar, *et al.*, In vivo Probabilistic Structural Atlas of the Inferior and Superior Colliculi, Medial and Lateral Geniculate Nuclei and Superior Olivary Complex in Humans Based on 7 Tesla MRI. *Frontiers in Neuroscience* **13** (2019).

46. M. G. García-Gomar, *et al.*, Disruption of Brainstem Structural Connectivity in REM Sleep Behavior Disorder Using 7 Tesla Magnetic Resonance Imaging. *Mov Disord* **37**, 847–853 (2022).

47. K. Singh, *et al.*, Probabilistic Template of the Lateral Parabrachial Nucleus, Medial Parabrachial Nucleus, Vestibular Nuclei Complex, and Medullary Viscero-Sensory-Motor Nuclei Complex in Living Humans From 7 Tesla MRI. *Frontiers in Neuroscience* **13** (2020).

48. K. Singh, M. G. García-Gomar, M. Bianciardi, Probabilistic Atlas of the Mesencephalic Reticular Formation, Isthmic Reticular Formation, Microcellular Tegmental Nucleus, Ventral Tegmental Area Nucleus Complex, and Caudal–Rostral Linear Raphe Nucleus Complex in Living Humans from 7 Tesla Magnetic Resonance Imaging. *Brain Connectivity* **11**, 613–623 (2021).

49. K.-J. Bär, *et al.*, Functional connectivity and network analysis of midbrain and brainstem nuclei. *Neuroimage* **134**, 53–63 (2016).

50. J. K. Harting, M. F. Huerta, T. Hashikawa, D. P. van Lieshout, Projection of the mammalian superior colliculus upon the dorsal lateral geniculate nucleus: Organization of tectogeniculate pathways in nineteen species. *Journal of Comparative Neurology* **304**, 275–306 (1991).

51. L. A. Benevento, J. H. Fallon, The ascending projections of the superior colliculus in the rhesus monkey (Macaca mulatta). *J Comp Neurol* **160**, 339–361 (1975).

52. A. J. Beitz, The organization of afferent projections to the midbrain periaqueductal gray of the rat. *Neuroscience* **7**, 133–159 (1982).

53. J. P. Card, R. Y. Moore, Organization of lateral geniculate-hypothalamic connections in the rat. *Journal of Comparative Neurology* **284**, 135–147 (1989).

54. J. D. Mikkelsen, A neuronal projection from the lateral geniculate nucleus to the lateral hypothalamus of the rat demonstrated with Phaseolus vulgaris leucoagglutinin tracing. *Neuroscience Letters* **116**, 58–63 (1990).

55. D. J. Uhlrich, J. B. Cucchiaro, S. M. Sherman, The projection of individual axons from the parabrachial region of the brain stem to the dorsal lateral geniculate nucleus in the cat. *J. Neurosci.* **8**, 4565–4575 (1988).

56. C. Fillinger, I. Yalcin, M. Barrot, P. Veinante, Efferents of anterior cingulate areas 24a and 24b and midcingulate areas 24a′ and 24b′ in the mouse. *Brain Struct Funct* **223**, 1747–1778 (2018).

57. R. W. Rieck, M. F. Huerta, J. K. Harting, J. T. Weber, Hypothalamic and ventral thalamic projections to the superior colliculus in the cat. *J Comp Neurol* **243**, 249–265 (1986).

58. J. H. Fallon, R. Y. Moore, Superior colliculus efferents to the hypothalamus. *Neuroscience Letters* **14**, 265–270 (1979).

59. M. Wiberg, Reciprocal connections between the periaqueductal gray matter and other somatosensory regions of the cat mid brain: A possible mechanism of pain inhibition. *Upsala Journal of Medical Sciences* **97**, 37–47 (1992).

60. N. J. Gandhi, H. A. Katnani, Motor Functions of the Superior Colliculus. *Annu Rev Neurosci* **34**, 205–231 (2011).

61. T. Isa, E. Marquez-Legorreta, S. Grillner, E. K. Scott, The tectum/superior colliculus as the vertebrate solution for spatial sensory integration and action. *Current Biology* **31**, R741–R762 (2021).

62. K. A. Keay, P. Redgrave, P. Dean, Cardiovascular and respiratory changes elicited by stimulation of rat superior colliculus. *Brain Research Bulletin* **20**, 13–26 (1988).

63. N. Sahibzada, P. Dean, P. Redgrave, Movements resembling orientation or avoidance elicited by electrical stimulation of the superior colliculus in rats. *J. Neurosci.* **6**, 723–733 (1986).

64. A. Damasio, G. B. Carvalho, The nature of feelings: evolutionary and neurobiological origins. *Nat Rev Neurosci* **14**, 143–152 (2013).

65. A. Damasio, H. Damasio, D. Tranel, Persistence of Feelings and Sentience after Bilateral Damage of the Insula. *Cereb Cortex* **23**, 833–846 (2013).

66. A. Erişir, S. C. V. Horn, M. E. Bickford, S. M. Sherman, Immunocytochemistry and distribution of parabrachial terminals in the lateral geniculate nucleus of the cat: A comparison with corticogeniculate terminals. *Journal of Comparative Neurology* **377**, 535–549 (1997).

67. A. Erişir, S. C. Van Horn, S. M. Sherman, Relative numbers of cortical and brainstem inputs to the lateral geniculate nucleus. *PNAS* **94**, 1517–1520 (1997).

68. R. Y. Moore, R. Weis, M. M. Moga, Efferent projections of the intergeniculate leaflet and the ventral lateral geniculate nucleus in the rat. *Journal of Comparative Neurology* **420**, 398–418 (2000).

69. L. P. Morin, J. H. Blanchard, Forebrain connections of the hamster intergeniculate leaflet: Comparison with those of ventral lateral geniculate nucleus and retina. *Vis Neurosci* **16**, 1037–1054 (1999).

70. M.-A. Coulombe, N. Erpelding, A. Kucyi, K. D. Davis, Intrinsic functional connectivity of periaqueductal gray subregions in humans: PAG Subregional Functional Connectivity. *Hum. Brain Mapp.* **37**, 1514–1530 (2016).

71. J. E. Iglesias, *et al.*, Bayesian longitudinal segmentation of hippocampal substructures in brain MRI using subject-specific atlases. *NeuroImage* **141**, 542–555 (2016).

72. H. F. Waguespack, B. L. Aguilar, L. Malkova, P. A. Forcelli, Inhibition of the Deep and Intermediate Layers of the Superior Colliculus Disrupts Sensorimotor Gating in Monkeys. *Frontiers in Behavioral Neuroscience* **14** (2020).

73. M. B. Parent, S. Higgs, L. G. Cheke, S. E. Kanoski, Memory and eating: A bidirectional relationship implicated in obesity. *Neuroscience & Biobehavioral Reviews* **132**, 110–129 (2022).

74. A. B. Satpute, *et al.*, Identification of discrete functional subregions of the human periaqueductal gray. *PNAS* **110**, 17101–17106 (2013).

75. R. J. Morecraft, *et al.*, Cytoarchitecture and cortical connections of the anterior cingulate and adjacent somatomotor fields in the rhesus monkey. *Brain Res Bull* **87**, 457–497 (2012).

76. T. Chiba, T. Kayahara, K. Nakano, Efferent projections of infralimbic and prelimbic areas of the medial prefrontal cortex in the Japanese monkey, Macaca fuscata. *Brain Res* **888**, 83–101 (2001).

77. B. A. Vogt, D. N. Pandya, Cingulate cortex of the rhesus monkey: II. Cortical afferents. *J Comp Neurol* **262**, 271–289 (1987).

78. D. N. Pandya, G. W. Van Hoesen, M. M. Mesulam, Efferent connections of the cingulate gyrus in the rhesus monkey. *Exp Brain Res* **42**, 319–330 (1981).

79. T. Caliński, J. Harabasz, A dendrite method for cluster analysis: Communications in Statistics: Vol 3, No 1. *Communications in Statistics* **3**, 1–27 (1974).

80. M. P. van den Heuvel, O. Sporns, Rich-Club Organization of the Human Connectome. *J. Neurosci.* **31**, 15775–15786 (2011).

81. M. P. van den Heuvel, R. S. Kahn, J. Goñi, O. Sporns, High-cost, high-capacity backbone for global brain communication. *Proc Natl Acad Sci U S A* **109**, 11372–11377 (2012).

82. M. Bianciardi, *et al.*, In vivo functional connectome of human brainstem nuclei of the ascending arousal, autonomic, and motor systems by high spatial resolution 7-Tesla fMRI. *MAGMA* **29**, 451–462 (2016).

83. X. An, R. Bandler, D. Ongür, J. L. Price, Prefrontal cortical projections to longitudinal columns in the midbrain periaqueductal gray in macaque monkeys. *J Comp Neurol* **401**, 455–479 (1998).

84. L. Jasmin, A. Granato, P. T. Ohara, Rostral agranular insular cortex and pain areas of the central nervous system: A tract-tracing study in the rat. *Journal of Comparative Neurology* **468**, 425–440 (2004).

85. X. Liu, *et al.*, The Superior Colliculus: Cell Types, Connectivity, and Behavior. *Neurosci. Bull.* **38**, 1519–1540 (2022).

86. H. W. Chase, A. A. Grace, P. T. Fox, M. L. Phillips, S. B. Eickhoff, Functional differentiation in the human ventromedial frontal lobe: A data-driven parcellation. *Human Brain Mapping* **41**, 3266–3283 (2020).

87. F. Jin, P. Zheng, H. Liu, H. Guo, Z. Sun, Functional and anatomical connectivity-based parcellation of human cingulate cortex. *Brain and Behavior* **8**, e01070 (2018).

88. N. Palomero-Gallagher, *et al.*, Human Pregenual Anterior Cingulate Cortex: Structural, Functional, and Connectional Heterogeneity. *Cerebral Cortex (New York, NY)* **29**, 2552 (2019).

89. E. T. Rolls, *et al.*, Functional Connectivity of the Anterior Cingulate Cortex in Depression and in Health. *Cerebral Cortex* **29**, 3617–3630 (2019).

90. C. Yu, *et al.*, Functional segregation of the human cingulate cortex is confirmed by functional connectivity based neuroanatomical parcellation. *NeuroImage* **54**, 2571–2581 (2011).

91. F. Cauda, *et al.*, Functional connectivity of the insula in the resting brain. *NeuroImage* **55**, 8–23 (2011).

92. L. J. Chang, T. Yarkoni, M. W. Khaw, A. G. Sanfey, Decoding the Role of the Insula in Human Cognition: Functional Parcellation and Large-Scale Reverse Inference. *Cerebral Cortex* **23**, 739–749 (2013).

93. B. Deen, N. B. Pitskel, K. A. Pelphrey, Three Systems of Insular Functional Connectivity Identified with Cluster Analysis. *Cerebral Cortex* **21**, 1498–1506 (2011).

94. C. Kelly, *et al.*, A convergent functional architecture of the insula emerges across imaging modalities. *NeuroImage* **61**, 1129–1142 (2012).

95. K. Singh, *et al.*, Functional connectome of arousal and motor brainstem nuclei in living humans by 7 Tesla resting-state fMRI. *NeuroImage* **249**, 118865 (2022).

96. J. M. Groot, *et al.*, Echoes from Intrinsic Connectivity Networks in the Subcortex. *J. Neurosci.* **43**, 6609–6618 (2023).

97. L. P. Morin, J. H. Blanchard, Forebrain connections of the hamster intergeniculate leaflet: comparison with those of ventral lateral geniculate nucleus and retina. *Vis Neurosci* **16**, 1037–1054 (1999).

98. Q. Ren, A. C. Marshall, J. Kaiser, S. Schütz-Bosbach, Multisensory integration of anticipated cardiac signals with visual targets affects their detection among multiple visual stimuli. *NeuroImage* **262**, 119549 (2022).

99. V. Bazinet, R. Vos de Wael, P. Hagmann, B. C. Bernhardt, B. Misic, Multiscale communication in cortico-cortical networks. *Neuroimage* **243**, 118546 (2021).

100. D. Ongür, J. L. Price, The organization of networks within the orbital and medial prefrontal cortex of rats, monkeys and humans. *Cereb Cortex* **10**, 206–219 (2000).

101. S. Demeter, D. L. Rosene, G. W. van Hoesen, Interhemispheric pathways of the hippocampal formation, presubiculum, and entorhinal and posterior parahippocampal cortices in the rhesus monkey: The structure and organization of the hippocampal commissures. *Journal of Comparative Neurology* **233**, 30–47 (1985).

102. Y. Kobayashi, D. G. Amaral, Macaque monkey retrosplenial cortex: III. Cortical efferents. *Journal of Comparative Neurology* **502**, 810–833 (2007).

103. C. R. Olson, S. Y. Musil, Topographic organization of cortical and subcortical projections to posterior cingulate cortex in the cat: Evidence for somatic, ocular, and complex subregions. *Journal of Comparative Neurology* **324**, 237–260 (1992).

104. P. Y. Risold, R. H. Thompson, L. W. Swanson, The structural organization of connections between hypothalamus and cerebral cortex. *Brain Res Brain Res Rev* **24**, 197–254 (1997).

105. M. P. van den Heuvel, O. Sporns, An Anatomical Substrate for Integration among Functional Networks in Human Cortex. *J. Neurosci.* **33**, 14489–14500 (2013).

106. J. Zhang, *et al.*, Topography Impacts Topology: Anatomically Central Areas Exhibit a "High-Level Connector" Profile in the Human Cortex. *Cereb Cortex* **30**, 1357–1365 (2020).

107. R. S. Maior, *et al.*, A role for the superior colliculus in the modulation of threat responsiveness in primates: toward the ontogenesis of the social brain. *Reviews in the Neurosciences* **23**, 697–706 (2012).

108. T. L. Davidson, *et al.*, Hippocampal lesions impair retention of discriminative responding based on energy state cues. *Behavioral Neuroscience* **124**, 97–105 (2010).

109. J. L. Gauthier, D. W. Tank, A Dedicated Population for Reward Coding in the Hippocampus. *Neuron* **99**, 179-193.e7 (2018).

110. S. E. Kanoski, H. J. Grill, Hippocampus Contributions to Food Intake Control: Mnemonic, Neuroanatomical, and Endocrine Mechanisms. *Biological Psychiatry* **81**, 748–756 (2017).

111. E. E. Noble, *et al.*, Hypothalamus-hippocampus circuitry regulates impulsivity via melanin-concentrating hormone. *Nat Commun* **10**, 4923 (2019).

112. D. Zeithamova, B. D. Gelman, L. Frank, A. R. Preston, Abstract Representation of Prospective Reward in the Hippocampus. *J. Neurosci.* **38**, 10093–10101 (2018).

113. A. N. Suarez, C. M. Liu, A. M. Cortella, E. E. Noble, S. E. Kanoski, Ghrelin and orexin interact to increase meal size through a descending hippocampus to hindbrain signaling pathway. *Biol Psychiatry* **87**, 1001–1011 (2020).

114. C. Shaffer, L. F. Barrett, K. S. Quigley, Signal processing in the vagus nerve: Hypotheses based on new genetic and anatomical evidence. *Biological Psychology* **182**, 108626 (2023).

115. M. Brændholt, *et al.*, Breathing in waves: Understanding respiratory-brain coupling as a gradient of predictive oscillations. *Neuroscience & Biobehavioral Reviews* **152**, 105262 (2023).

116. H. C. Hughes, W. H. Mullikin, Brainstem afferents to the lateral geniculate nucleus of the cat. *Exp Brain Res* **54** (1984).

117. J. K. Ruffle, *et al.*, The autonomic brain: Multi-dimensional generative hierarchical modelling of the autonomic connectome. *Cortex* **143**, 164–179 (2021).

118. F. De la Cruz, *et al.*, Central Autonomic Network Alterations in Anorexia Nervosa Following Peripheral Adrenergic Stimulation. *Biol Psychiatry Cogn Neurosci Neuroimaging* **8**, 720–730 (2023).

119. J. Shao, *et al.*, Common and distinct changes of default mode and salience network in schizophrenia and major depression. *Brain Imaging Behav* **12**, 1708–1719 (2018).

120. R. Li, *et al.*, Dissociable salience and default mode network modulation in generalized anxiety disorder: a connectome-wide association study. *Cereb Cortex* **33**, 6354–6365 (2023).

121. L. F. Barrett, K. S. Quigley, P. Hamilton, An active inference theory of allostasis and interoception in depression. *Philos Trans R Soc Lond B Biol Sci* **371**, 20160011 (2016).

122. C. Shaffer, C. Westlin, K. S. Quigley, S. Whitfield-Gabrieli, L. F. Barrett, Allostasis, Action, and Affect in Depression: Insights from the Theory of Constructed Emotion. *Annu Rev Clin Psychol* **18**, 553–580 (2022).

123. M. Ardizzi, *et al.*, Interoception and Positive Symptoms in Schizophrenia. *Frontiers in Human Neuroscience* **10** (2016).

124. B. Yao, K. Thakkar, Interoception abnormalities in schizophrenia: A review of preliminary evidence and an integration with Bayesian accounts of psychosis. *Neurosci Biobehav Rev* **132**, 757–773 (2022).

125. D. DuBois, S. H. Ameis, M.-C. Lai, M. F. Casanova, P. Desarkar, Interoception in Autism Spectrum Disorder: A review. *International Journal of Developmental Neuroscience* **52**, 104–111 (2016).

126. K. B. Schauder, L. E. Mash, L. K. Bryant, C. J. Cascio, Interoceptive ability and body awareness in autism spectrum disorder. *Journal of Experimental Child Psychology* **131**, 193–200 (2015).

127. I. García-Cordero, *et al.*, Feeling, learning from and being aware of inner states: interoceptive dimensions in neurodegeneration and stroke. *Philosophical Transactions of the Royal Society B: Biological Sciences* **371**, 20160006 (2016).

128. C. R. Marshall, *et al.*, Impaired Interoceptive Accuracy in Semantic Variant Primary Progressive Aphasia. *Frontiers in Neurology* **8** (2017).

129. L. Ricciardi, *et al.*, Know thyself: Exploring interoceptive sensitivity in Parkinson's disease. *Journal of the Neurological Sciences* **364**, 110–115 (2016).

130. G. Santangelo, *et al.*, Interoceptive processing deficit: A behavioral marker for subtyping Parkinson's disease. *Parkinsonism & Related Disorders* **53**, 64–69 (2018).

131. A. Yoris, *et al.*, Multicentric evidence of emotional impairments in hypertensive heart disease. *Sci Rep* **10**, 14131 (2020).

132. D. Di Lernia, M. Lacerenza, V. Ainley, G. Riva, Altered Interoceptive Perception and the Effects of Interoceptive Analgesia in Musculoskeletal, Primary, and Neuropathic Chronic Pain Conditions. *Journal of Personalized Medicine* **10**, 201 (2020).

133. B. Bonaz, *et al.*, Diseases, Disorders, and Comorbidities of Interoception. *Trends in Neurosciences* **44**, 39–51 (2021).

134. S. S. Khalsa, *et al.*, Interoception and Mental Health: A Roadmap. *Biol Psychiatry Cogn Neurosci Neuroimaging* **3**, 501–513 (2018).

135. G. Locatelli, *et al.*, What is the role of interoception in the symptom experience of people with a chronic condition? A systematic review. *Neuroscience & Biobehavioral Reviews* **148**, 105142 (2023).

136. J. P. Hamilton, M. Farmer, P. Fogelman, I. H. Gotlib, Depressive Rumination, the Default-Mode Network, and the Dark Matter of Clinical Neuroscience. *Biological Psychiatry* **78**, 224–230 (2015).

137. H.-X. Zhou, *et al.*, Rumination and the default mode network: Meta-analysis of brain imaging studies and implications for depression. *NeuroImage* **206**, 116287 (2020).

138. L. Q. Uddin, *et al.*, Salience Network–Based Classification and Prediction of Symptom Severity in Children With Autism. *JAMA Psychiatry* **70**, 869–879 (2013).

139. M. N. Baliki, A. R. Mansour, A. T. Baria, A. V. Apkarian, Functional Reorganization of the Default Mode Network across Chronic Pain Conditions. *PLOS ONE* **9**, e106133 (2014).

140. H. Chen, *et al.*, Shared atypical default mode and salience network functional connectivity between autism and schizophrenia. *Autism Research* **10**, 1776–1786 (2017).

141. S. C. de Lange, *et al.*, Shared vulnerability for connectome alterations across psychiatric and neurological brain disorders. *Nat Hum Behav* **3**, 988–998 (2019).

142. G. E. Doucet, *et al.*, Transdiagnostic and disease-specific abnormalities in the default-mode network hubs in psychiatric disorders: A meta-analysis of resting-state functional imaging studies. *European Psychiatry* **63**, e57 (2020).

143. C.-C. Huang, *et al.*, Transdiagnostic and Illness-Specific Functional Dysconnectivity Across Schizophrenia, Bipolar Disorder, and Major Depressive Disorder. *Biological Psychiatry: Cognitive Neuroscience and Neuroimaging* **5**, 542–553 (2020).

144. C. L. Nord, S. N. Garfinkel, Interoceptive pathways to understand and treat mental health conditions. *Trends in Cognitive Sciences* **26**, 499–513 (2022).

145. C. C. C. Bauer, *et al.*, Real-time fMRI neurofeedback reduces auditory hallucinations and modulates resting state connectivity of involved brain regions: Part 2: Default mode network -preliminary evidence. *Psychiatry Res* **284**, 112770 (2020).

146. J. Zhang, *et al.*, Reducing default mode network connectivity with mindfulness-based fMRI neurofeedback: a pilot study among adolescents with affective disorder history. *Mol Psychiatry* 1–9 (2023). https://doi.org/10.1038/s41380-023-02032-z.

147. J. Cesario, D. J. Johnson, H. L. Eisthen, Your Brain Is Not an Onion With a Tiny Reptile Inside. *Curr Dir Psychol Sci* **29**, 255–260 (2020).

148. L. Chanes, L. F. Barrett, Redefining the Role of Limbic Areas in Cortical Processing. *Trends in Cognitive Sciences* **20**, 96–106 (2016).

149. T. Nakai, S. Nishimoto, Representations and decodability of diverse cognitive functions are preserved across the human cortex, cerebellum, and subcortex. *Commun Biol* **5**, 1–13 (2022).

150. M. M. Mesulam, From sensation to cognition. *Brain* **121**, 1013–1052 (1998).

151. C. L. Zold, M. G. H. Shuler, Theta Oscillations in Visual Cortex Emerge with Experience to Convey Expected Reward Time and Experienced Reward Rate. *J. Neurosci.* **35**, 9603–9614 (2015).

152. A. B. Satpute, *et al.*, Involvement of Sensory Regions in Affective Experience: A Meta-Analysis. *Front Psychol* **6**, 1860 (2015).

153. P. Vuilleumier, How brains beware: neural mechanisms of emotional attention. *Trends Cogn Sci* **9**, 585–594 (2005).

154. M. Allen, *et al.*, Anterior insula coordinates hierarchical processing of tactile mismatch responses. *Neuroimage* **127**, 34–43 (2016).

155. T. Engelen, M. Solcà, C. Tallon-Baudry, Interoceptive rhythms in the brain. *Nat Neurosci* **26**, 1670–1684 (2023).

156. E. Houldin, Z. Fang, L. B. Ray, A. M. Owen, S. M. Fogel, Toward a complete taxonomy of resting state networks across wakefulness and sleep: an assessment of spatially distinct resting state networks using independent component analysis. *Sleep* **42**, zsy235 (2019).

157. S. G. Horovitz, *et al.*, Decoupling of the brain's default mode network during deep sleep. *Proc Natl Acad Sci U S A* **106**, 11376–11381 (2009).

158. E. Tagliazucchi, H. Laufs, Decoding wakefulness levels from typical fMRI resting-state data reveals reliable drifts between wakefulness and sleep. *Neuron* **82**, 695–708 (2014).

159. S. Titone, *et al.*, Frequency-dependent connectivity in large-scale resting-state brain networks during sleep. *Eur J Neurosci* **59**, 686–702 (2024).

160. C. Korponay, A. C. Janes, B. B. Frederick, Brain-wide functional connectivity artifactually inflates throughout functional magnetic resonance imaging scans. *Nat Hum Behav* **8**, 1568–1580 (2024).

161. M. Tsanov, Differential and complementary roles of medial and lateral septum in the orchestration of limbic oscillations and signal integration. *European Journal of Neuroscience* **48**, 2783–2794 (2018).

162. Y. Takeuchi, *et al.*, The Medial Septum as a Potential Target for Treating Brain Disorders Associated With Oscillopathies. *Frontiers in Neural Circuits* **15** (2021).

163. G. T. Cottrell, A. V. Ferguson, Sensory circumventricular organs: central roles in integrated autonomic regulation. *Regulatory Peptides* **117**, 11–23 (2004).

164. C. J. Price, T. D. Hoyda, A. V. Ferguson, The area postrema: a brain monitor and integrator of systemic autonomic state. *Neuroscientist* **14**, 182–194 (2008).

165. M. A. Karim, S. K. Leong, S. A. Perwaiz, On the anatomical organization of the vagal nuclei. *American Journal of Primatology* **1**, 277–292 (1981).

166. M. Kalia, M. M. Mesulam, Brain stem projections of sensory and motor components of the vagus complex in the cat: II. Laryngeal, tracheobronchial, pulmonary, cardiac, and gastrointestinal branches. *J Comp Neurol* **193**, 467–508 (1980).

167. T. Osada, *et al.*, Functional subdivisions of the hypothalamus using areal parcellation and their signal changes related to glucose metabolism. *NeuroImage* **162**, 1–12 (2017).

168. D. E. A. Jensen, K. P. Ebmeier, S. Suri, M. F. S. Rushworth, M. C. Klein-Flügge, Nuclei-specific hypothalamus networks predict a dimensional marker of stress in humans. *Nat Commun* **15**, 2426 (2024).

169. J.-N. Zhu, J.-J. Wang, The cerebellum in feeding control: possible function and mechanism. *Cell Mol Neurobiol* **28**, 469–478 (2008).

170. J.-N. Zhu, W.-H. Yung, B. Kwok-Chong Chow, Y.-S. Chan, J.-J. Wang, The cerebellar-hypothalamic circuits: potential pathways underlying cerebellar involvement in somatic-visceral integration. *Brain Res Rev* **52**, 93–106 (2006).

171. J. D. Power, K. A. Barnes, A. Z. Snyder, B. L. Schlaggar, S. E. Petersen, Spurious but systematic correlations in functional connectivity MRI networks arise from subject motion. *Neuroimage* **59**, 2142–2154 (2012).

172. I. R. Kleckner, *et al.*, Evidence for a large-scale brain system supporting allostasis and interoception in humans. *Nat Hum Behav* **1**, 1–14 (2017).

173. J. E. Iglesias, *et al.*, A computational atlas of the hippocampal formation using ex vivo, ultra-high resolution MRI: Application to adaptive segmentation of in vivo MRI. *Neuroimage* **115**, 117–137 (2015).

174. A. L. Cohen, *et al.*, Defining functional areas in individual human brains using resting functional connectivity MRI. *Neuroimage* **41**, 45–57 (2008).

175. T. Yarkoni, Big Correlations in Little Studies: Inflated fMRI Correlations Reflect Low Statistical Power-Commentary on Vul et al. (2009). *Perspect Psychol Sci* **4**, 294–298 (2009).

176. L. J. Cronbach, N. Rajaratnam, G. C. Gleser, Theory of generalizability: A liberalization of reliability theory. *British Journal of Statistical Psychology* **16**, 137–163 (1963).

177. M. Xia, J. Wang, Y. He, BrainNet Viewer: A Network Visualization Tool for Human Brain Connectomics. *PLOS ONE* **8**, e68910 (2013).

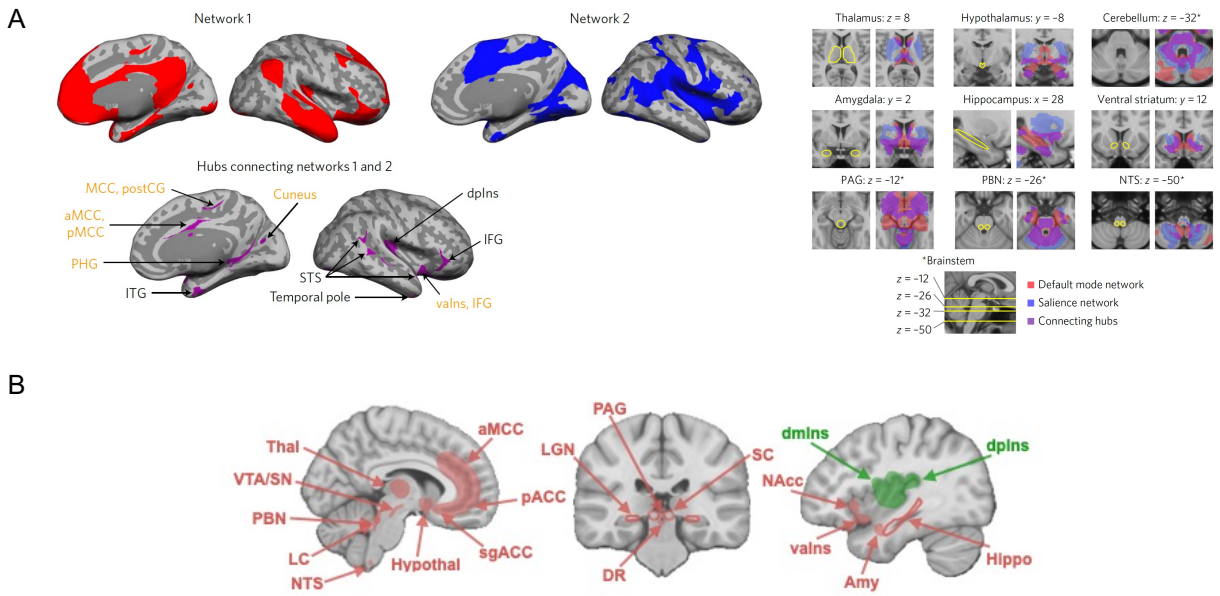

Figure 1. Key cortical and subcortical regions involved in interoception and allostasis. **(A)** Using 3 Tesla fMRI resting state connectivity, we showed a unified system consisting of the default mode network (in red) and salience network (in blue), which overlapped in many key cortical visceromotor allostatic regions (in purple) that also serve as 'rich club' hubs, in addition to a portion of primary interoceptive cortex (dpIns) (left panel) (19). We reported the system's connectivity to some subcortical regions known to play a role in control of the autonomic nervous system, the immune system, and the endocrine system such as the thalamus, hypothalamus, hippocampus, ventral striatum, PAG, PBN and NTS (e.g., 20–26) (right panel) (19). Figures are reproduced with permission from (19). (B) Expanded set of seed regions used in the present analysis. Abbreviations: aMCC: anterior midcingulate cortex; Amy: amygdala; dmIns: dorsal mid insula; dpIns: dorsal posterior insula; DR: dorsal raphe; Hippo: hippocampus; Hypothal: hypothalamus; LC: locus coeruleus; LGN: lateral geniculate nucleus; NAcc: nucleus accumbens; NTS: nucleus of the solitary tract; pACC: pregenual anterior cingulate cortex; PAG: periaqueductal gray; PBN: parabrachial nucleus; SC: superior colliculus; sgACC: subgenual anterior cingulate cortex; SN: substantia nigra; Thal: thalamus; vaIns: ventral anterior insula; VTA: ventral tegmental area.

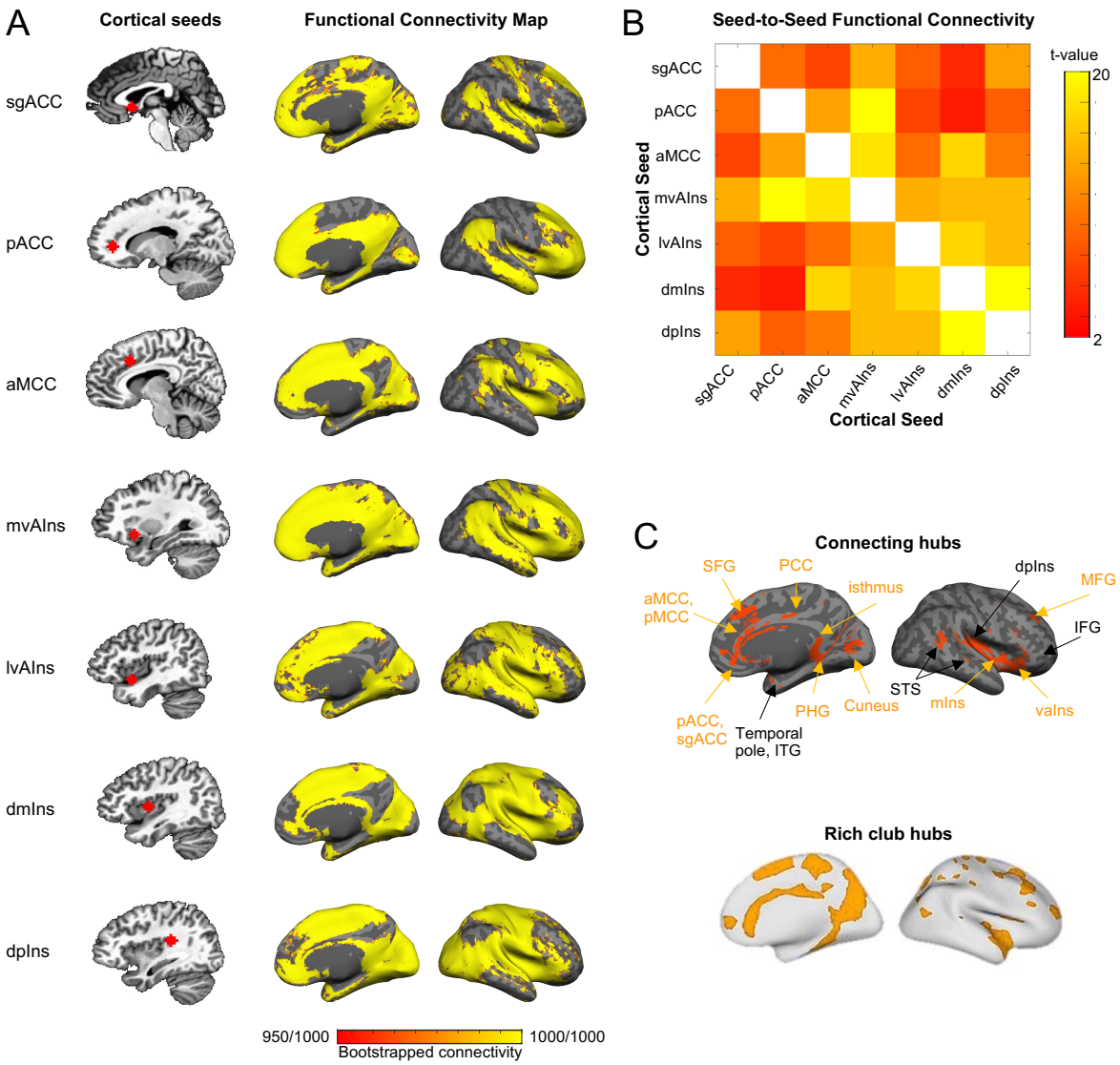

Figure 2. Cortico-cortical functional connectivity within the allostatic-interoceptive system. **(A)** Left column shows cortical seed locations and right column shows bootstrapped functional connectivity maps depicting all voxels whose time course was correlated ($p < .05$) with that of the seed in more than 950 iterations (out of 1000) by resampling 80% of the sample in each iteration ($N = 72$). **(B)** Seed-to-seed functional connectivity matrix shows connectivity strength between each pair of the cortical seeds ($p < .05$, uncorrected; white color indicates correlation =1; $N = 90$). **(C)** The allostatic-interoceptive system showed connecting regions in all the *a priori* interoceptive and visceromotor control regions. Connecting regions belonging to the 'rich club' are labeled in yellow. 'Rich club' hubs figure adapted with permission from (105). To avoid Type II errors, which are enhanced with the use of stringent statistical thresholds (175), we opted to separate signal from random noise using replication, according to the mathematics of classical measurement theory (176). Abbreviations: aMCC: anterior mid cingulate cortex; dpIns: dorsal posterior insula; IFG: inferior frontal gyrus; MFG: middle frontal gyrus; mIns: mid insula; pACC: pregenual anterior cingulate cortex; PHG: parahippocampal gyrus; pMCC: posterior mid cingulate cortex; PCC: posterior cingulate cortex; sgACC: subgenual anterior cingulate cortex; STS: superior temporal sulcus; vaIns: ventral anterior insula.

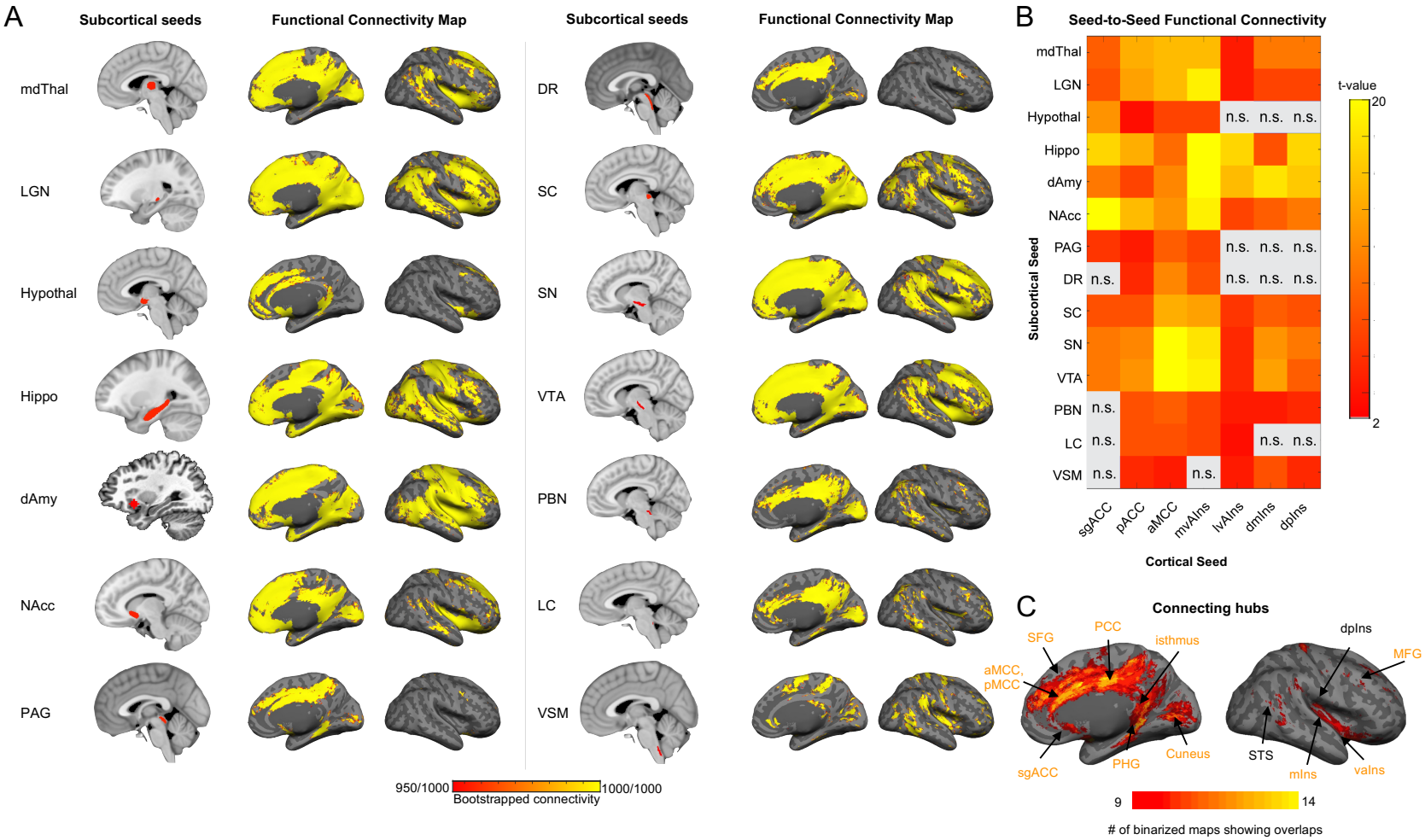

Figure 3. Subcortico-cortical intrinsic connectivity within the allostatic-interoceptive system. **(A)** Left column shows subcortical seed locations and right column shows bootstrapped functional connectivity discovery maps depicting all cortical voxels whose time course was correlated ($p < .05$) with that of the seed in more than 950 iterations (out of 1000) by resampling 80% of the sample in each iteration ($N = 72$). **(B)** Seed-to-seed functional connectivity matrix shows connectivity strength between pairs of subcortical and cortical seeds ($p < .05$, uncorrected; gray color indicates subthreshold correlations; $N = 90$). **(C)** Conjunction map shows the number of binarized maps ($p < .05$) with shared connecting regions (ranging from 9 to 14). Abbreviations: dAmy: dorsal amygdala; mdThal: mediodorsal thalamus; LGN: lateral geniculate nucleus; Hypothal: hypothalamus; Hippo: hippocampus; NAcc: nucleus accumbens; PAG: periaqueductal gray;

DR: dorsal raphe; SC: superior colliculus; SN: substantia nigra; VTA: ventral tegmental area; PBN: parabrachial nucleus; LC: locus coeruleus; VSM: medullary viscero-sensory-motor nuclei complex corresponding to the nucleus tractus solitarius.

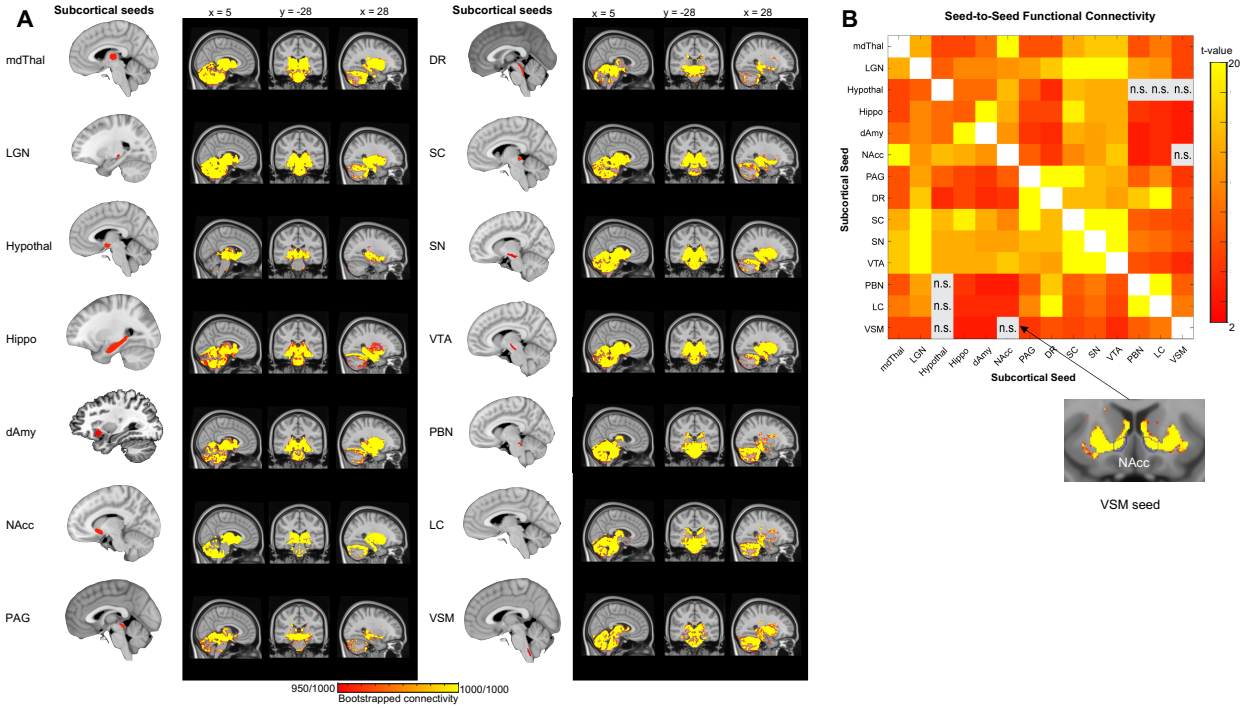

Figure 4. Subcortico-subcortical intrinsic connectivity within the allostatic-interoceptive system. **(A)** Left column shows subcortical seed locations and right column shows bootstrapped functional connectivity discovery maps depicting all subcortical voxels whose time course was correlated ($p < .05$) with that of the seed in more than 950 iterations (out of 1000) by resampling 80% of the sample in each iteration ($N = 72$). **(B)** Seed-to-seed functional connectivity matrix showed connectivity strength between each pair of the subcortical seeds ($p < .05$, uncorrected; white color indicates correlation =1 and gray color indicates subthreshold correlations; $N = 90$). Several seeds had functional connectivity with a subset of voxels within target ROIs, as shown by binarized maps at $p < .05$ (target ROI outline is shown in blue).

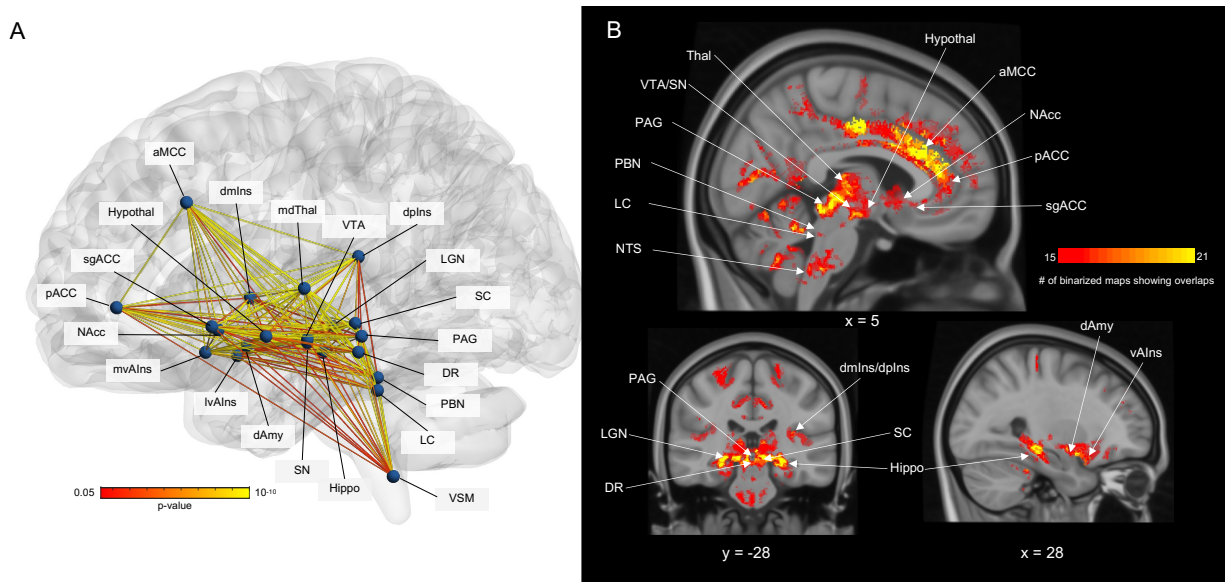

Figure 5. Summary of the allostatic-interoceptive system based on 7 Tesla fMRI functional connectivity. **(A)** Circuit diagram indicates dense within-system connectivity between the 21 cortical and subcortical seeds. All seeds are shown as spherical nodes located at their respective centers of gravity. Pairwise connectivity strengths between ROIs are shown as edges between nodes (ranging from $p < .05$ in red to $p < 10^{-10}$ in yellow, uncorrected; $N = 90$). Nodes and edges in the glass brain were visualized using BrainNet Viewer (177) **(B)** Conjunction map shows the number of binarized maps ($p < .05$) that shared overlapping regions (ranging from 15 to 21, total number of cortical and subcortical seeds = 21).